The Astrophysical Journal, 839:84 (7pp), 2017 April 20 https://doi.org/10.3847/1538-4357/aa6796

High-energy Gamma-Ray Activity from V404 Cygni Detected by *AGILE* during the 2015 June Outburst

G. Piano[1], P. Munar-Adrover[1], F. Verrecchia[2,3], M. Tavani[1,4,5], and S. A. Trushkin[6,7]
[1] INAF-IAPS, Via del Fosso del Cavaliere 100, I-00133 Roma, Italy; giovanni.piano@iaps.inaf.it
[2] ASI Data Center (ASDC), Via del Politecnico snc, I-00133 Roma, Italy
[3] INAF-OAR, Via di Frascati 33, I-00040 Monte Porzio Catone (RM), Italy
[4] INFN Roma Tor Vergata, Via della Ricerca Scientifica 1, I-00133 Roma, Italy
[5] Dipertimento di Fisica, Università di Roma "Tor Vergata", Via Orazio Raimondo 18, I-00173 Roma, Italy
[6] Special Astrophysical Observatory RAS, Karachaevo-Cherkassian Republic, Nizhnij Arkhyz 36916, Russia
[7] Kazan Federal University, Kazan 420008, Russia
Received 2016 November 21; revised 2017 March 7; accepted 2017 March 9; published 2017 April 18

Abstract

The *AGILE* satellite detected transient high-energy γ-ray emission from the X-ray binary V404 Cygni, during the 2015 June outburst observed in radio, optical, X-ray, and soft γ-ray frequencies. The activity was observed by *AGILE* in the 50–400 MeV energy band, between 2015 June 24 UT 06:00:00 and 2015 June 26 UT 06:00:00 (MJD 57197.25–57199.25), with a detection significance of $\sim 4.3\sigma$. The γ-ray detection, consistent with a contemporaneous observation by *Fermi*-LAT, is correlated with a bright flare observed at radio and hard X-ray frequencies, and with a strong enhancement of the 511 keV line emission, possibly indicating plasmoid ejections in a lepton-dominated transient jet. The *AGILE* observations of this binary system are compatible with a microquasar scenario in which transient jets are responsible for the high-energy γ-ray emission.

Key words: gamma rays: stars – stars: black holes – stars: jets – X-rays: binaries

Supporting material: tar.gz file

1. Introduction

V404 Cygni (hereafter V404 Cyg), also known as GS 2023 +338, is a low mass X-ray binary (LMXB) located at a distance of 2.39 ± 0.14 kpc, accurately inferred by a parallax measurement (Miller-Jones et al. 2009). The system is composed of a $9^{+0.2}_{-0.6}\,M_{\odot}$ black hole (BH) and a $0.7^{+0.3}_{-0.2}\,M_{\odot}$ K3 III companion star with an orbital period of 6.4714 ± 0.0001 days (Casares et al. 1992) and a 67° inclination with respect to the line of sight (Casares & Charles 1994; Shahbaz et al. 1994; Khargharia et al. 2010). V404 Cyg was discovered as a nova during an optical outburst in 1938, and it was observed for the first time in the X-ray band by the GINGA satellite, during an intense outburst in 1989 (Makino et al. 1989).

LMXBs are usually transient systems, showing long periods of quiescence (years), with faint and rapidly variable emission in the X-ray and radio frequencies (Miller-Jones et al. 2008; Hynes et al. 2009; Rana et al. 2016) and bright outburst states (weeks/months). The X-ray luminosities span from 10^{31-33} erg s^{-1} during quiescence phase up to Eddington limit ($L_{\rm Edd} \approx 10^{39}$ erg s^{-1} for a $9\,M_{\odot}$ BH) in the outburst states (Rodriguez et al. 2015).

After a quiescence period of ~26 years, the detection by *Swift*/BAT triggered the observations of a new active phase on 2015 June 15 (MJD 57188; Barthelmy et al. 2015) that lasted ~2 weeks and was observed across all wavelengths (from radio to soft γ-rays), with a highly variable emission (Rodriguez et al. 2015; Trushkin et al. 2015; Jenke et al. 2016). The correlated variability between optical and X-ray emissions during the bright 2015 June activity has been interpreted as a consequence of the instability of its large accretion disk (the outer accretion disk radius is $R_{\rm out} \sim 10^7$ km). A disruption of the accreting mass inflow into the inner part of the disk can represent a critical factor to explain the observed scenario of this intense outburst: large-amplitude fluctuations that rapidly ended after only two weeks. The outburst possibly started in the innermost part of the disk, but it was not sustained by the accretion. The mass inflow could be disrupted either by a low surface density in the outer part of the disk—because of its long orbital period (Kimura et al. 2016)—or by a strong outer-disk wind regulating the accretion (Muñoz-Darias et al. 2016).

In 2015 June, besides optical and X-ray intense variable emissions, indicating the combined activity of the corona–disk system, observations in radio (Trushkin et al. 2015) and γ-ray energies (Loh et al. 2016; Siegert et al. 2016) confirmed the ejection of relativistic plasma jets. In particular, hints of e^+ e^- pair annihilation, which are consistent with a microquasar scenario, have been found by *INTEGRAL* during the active phase (Siegert et al. 2016).

In this paper, we present the *AGILE* observations of V404 Cyg during the peak phase of this intense activity, compare the results with the *Fermi*-LAT data, and analyze the high-energy (HE) γ-ray emission in a multiwavelength context.

2. Observations and Data Analysis

We analyzed the data collected by the Gamma-Ray Imaging Detector (GRID; Barbiellini et al. 2002; Prest et al. 2003), the γ-ray silicon-tracker imager on board the *AGILE* satellite (for a detailed description of the *AGILE* payload, see Tavani et al. 2009a), and we compared our results with the *Fermi*-LAT observations of the system (see the Appendix).

The *AGILE*-GRID is sensitive to γ-ray photons in the energy range 30 MeV–30 GeV. The point-spread function (PSF) at 100 and 400 MeV is 4.°2 and 1.°2 (68% containment radius), respectively (Sabatini et al. 2015). *AGILE* had operated in a "pointing" mode of data-taking, characterized by fixed attitude observations, until 2009 November, when the satellite entered

in "spinning" mode, covering a large fraction of the sky with a controlled rotation of the pointing axis. In this current observing mode, typical two-day integration-time sensitivity (3σ) for sources in the Galactic plane and photon energy above 100 MeV is $\sim 10^{-6}$ photons cm^{-2} s^{-1}.

The analysis of the *AGILE*-GRID data was carried out with the new `Build_23` scientific software, `FM3.119` calibrated filter, and `I0025` response matrices. The consolidated archive, available from the ASI Data Center (`ASDCSTDk`), was analyzed by applying South Atlantic Anomaly event cuts and 80° Earth albedo filtering. Only incoming γ-ray events with an off-axis angle lower than 60° were selected for the analysis. Statistical significance and flux determination of the point sources were calculated by using the *AGILE* multi-source likelihood analysis (MSLA) software (Bulgarelli et al. 2012) based on the Test Statistic (TS) method as formulated by Mattox et al. (1996). This statistical approach provides a detection significance assessment of a γ-ray source by comparing maximum-likelihood values of the null hypothesis (no source in the model) with the alternative hypothesis (point source in the field model). In this work, we report 68% confidence level (C. L.) flux upper limits (ULs) if TS < 9 (detection significance $\lesssim 3$) and flux values with the corresponding 1σ statistical errors otherwise (TS $\geqslant 9$).

Before analyzing the outburst interval, we carried out an analysis of the Cygnus field during a five-month period between 2015 January 01 UT 12:00:00 and 2015 June 01 UT 12:00:00. The analysis took into account two different energy bands: 50–400 MeV and above 400 MeV. This preliminary analysis allowed us to model the γ-ray field just before the onset of the strong activity from V404 Cyg. For both energy ranges we performed an MSLA including—in addition to V404 Cyg—the three main pulsars of the Cygnus region (PSR J2021+3651, PSR J2021+4026, and PSR J2032+4127), which are known to be intense and persistent γ-ray sources. We modeled the γ-ray spectrum for V404 Cyg by assuming a simple power law with a 2.1 photon index.[8] Flux ULs of 1×10^{-7} photons cm^{-2} s^{-1}and 2×10^{-8} photons cm^{-2} s^{-1} were found for V404 Cyg in 50–400 MeV and >400 MeV energy bands, respectively. The fluxes of the three γ-ray pulsars, found in these five-month preliminary analyses, were kept fixed in the following MSLAs for the outburst phase. Furthermore, the diffuse emission (Galactic and extragalactic) quantified in this preliminary analysis was kept fixed during the study of the active period (2015 June).

For the outburst activity period we analyzed the time interval from 2015 June 20 UT 06:00:00 to 2015 June 30 UT 06:00:00, across the giant flare recorded by *Swift*/BAT (Segreto et al. 2015) and RATAN-600 (Trushkin et al. 2015) on 2015 June 26 (MJD 57199). A 48 hr bin light curve for V404 Cyg was calculated (with an MSLA approach) in both energy bands. We selected these periods (five 48 hr time intervals) in order to ensure a stable exposure for the target source. In the 50–400 MeV energy band, the on-source exposure for each bin was found to be almost constant around a value of $\sim 5.16 \times 10^6$ cm^2 s with a mean fluctuation of ~3%. No detection with TS > 9 was found in the >400 MeV energy band, with 48 hr flux ULs lower than 5×10^{-7} photons cm^{-2} s^{-1}.

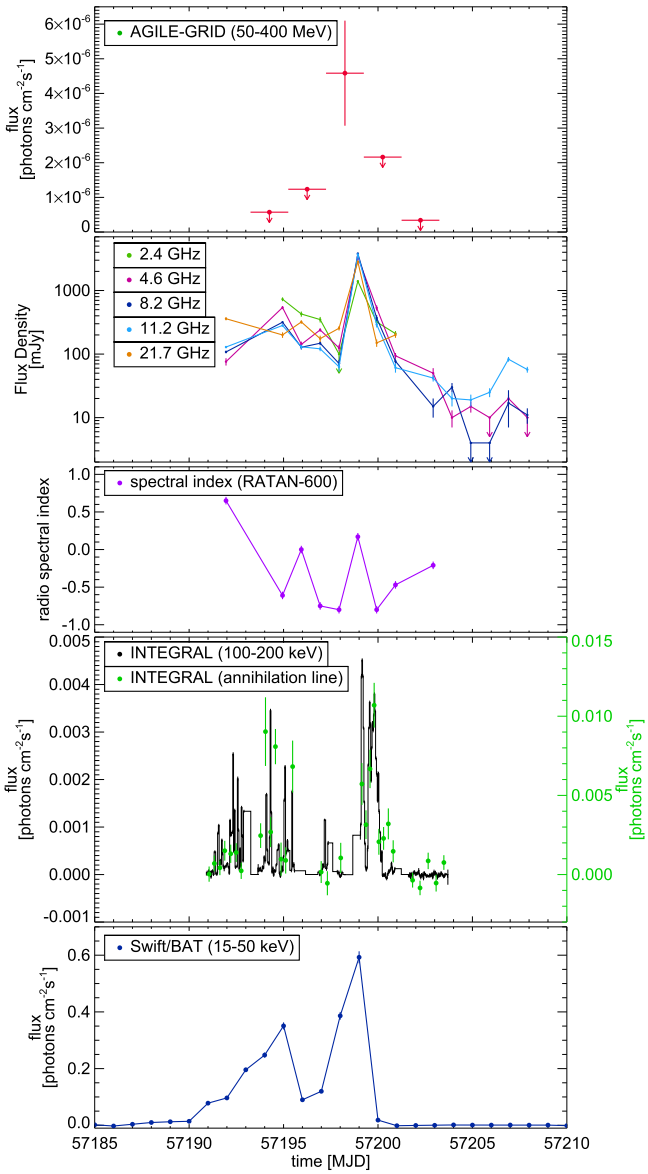

Figure 1. Multiwavelength light curve throughout the 2015 June outburst of V404 Cyg. From top to bottom: *AGILE*-GRID 50–400 MeV, 48 hr integration; RATAN-600 radio flux density (2.4, 4.6, 8.2, 11.2, and 21.7 GHz); RATAN-600 radio spectral index (4–11 GHz); *INTEGRAL*/SPI continuum (100–200 keV, black histogram) and annihilation line (green points), data from Siegert et al. (2016); *Swift*/BAT 15–50 keV, one-day bin.

In the 50–400 MeV energy band, a detection was found in the time interval between 2015 June 24 UT 06:00:00 and 2015 June 26 UT 06:00:00 (MJD 57197.25–57199.25), at Galactic coordinates $(l, b) = (72.^\circ41, -2.^\circ75) \pm 0.^\circ97$ (stat.) $\pm$ $0.^\circ10$ (syst.), with TS = 18.1 ($\sim 4.3\sigma$) and a γ-ray flux $F_\gamma = (4.6 \pm 1.5) \times 10^{-6}$ photons cm^{-2} s^{-1} (see Figures 1 and 6).[9] In the left panel of Figure 2, the corresponding *AGILE*-GRID γ-ray intensity map is shown, with the result of the best-fitting position. The nominal position of V404 Cyg is within the error ellipse of the *AGILE* γ-ray excess. The time correlation with the peak outburst phase observed in other wavelengths gives robustness to the association with V404 Cyg

[8] This is a standard value used in the *AGILE* analysis for unknown-spectrum or low-statistics sources (see Pittori et al. 2009).

[9] The systematic errors on flux measurements for *AGILE* have been quantified in 10% of the total.

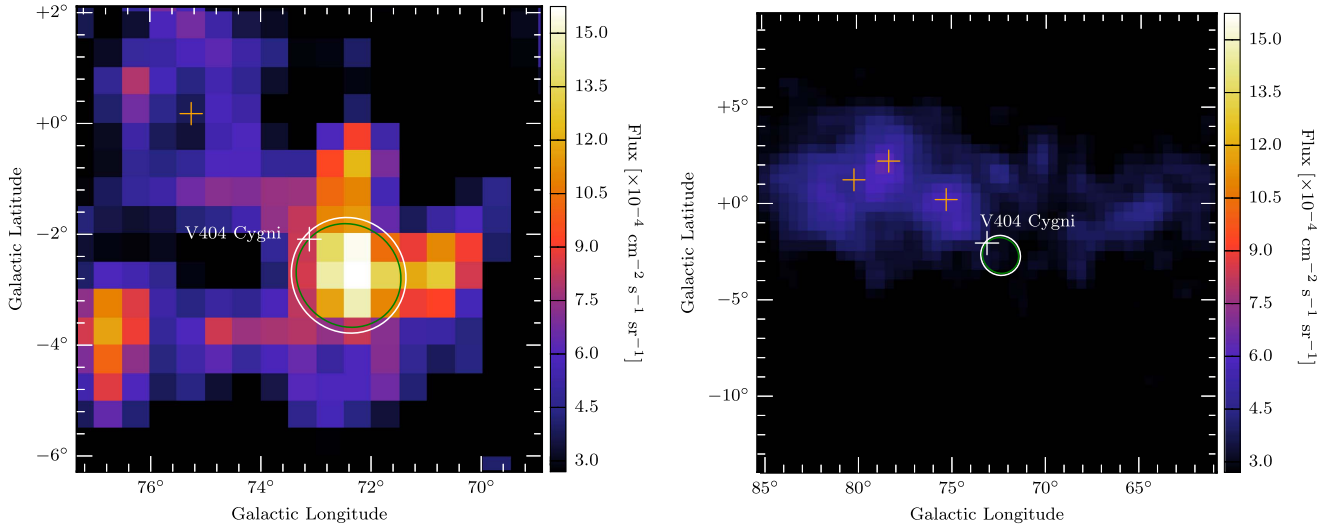

Figure 2. Left panel: *AGILE*-GRID γ-ray intensity map in Galactic coordinates with a three-pixel Gaussian smoothing. Photon energy: 50–400 MeV. Integration time: 2015 June 20 UT 06:00:00–2015 June 30 UT 06:00:00. Pixel size: 0.°5. Green contour: 95% confidence region. White contour: statistical + systematic (0.°1) containment region. White cross: optical position of V404 Cyg. Right panel: the quiescent phase of V404 Cyg—with the same characteristics as the left panel, but a different size—from 2015 January 1 UT 12:00:00 to 2015 June 1 UT 12:00:00. The three pulsars included in the multi-source analysis are marked with magenta crosses (from left to right: PSR J2032+4127, PSR J2021+4026, and PSR J2021+3651). The white cross is the optical position of V404 Cyg. The white contour is the *AGILE* containment region of the flaring source (stat + syst). The color bar is the same for both the maps.

(see Section 3.1). For comparison, the right panel shows the quiescent phase of V404 Cyg as detected between 2015 January 1 UT 12:00:00 and 2015 June 1 UT 12:00:00.

In Figure 3, the *AGILE* differential γ-ray spectrum (50 MeV–1 GeV) for V404 Cyg during the 48 hr peak activity is shown. No significant γ-ray emission is detected above 400 MeV.

The γ-ray peak emission detected by *AGILE* is compatible in time with our analysis of *Fermi*-LAT data (TS = 13.4, MJD 57198.75–59199.75) in the 60–400 MeV energy band. Furthermore, our findings are consistent with the *Fermi*-LAT observations published in Loh et al. (2016). For a detailed description of our independent *Fermi*-LAT data analysis see the Appendix. A comparison between the *AGILE*-GRID and *Fermi*-LAT observations and findings is presented in Appendix A.1.

3. Discussion

3.1. AGILE Results in a Multiwavelength Context

In Figure 1, we plotted the *AGILE*-GRID light curve together with published data from RATAN-600 (Trushkin et al. 2015), *INTEGRAL*/SPI (Siegert et al. 2016), and *Swift*/BAT.[10] A plot showing the time evolution of the radio spectral index α (where $S \sim \nu^{\alpha}$ is the radio flux density), in the band 4–11 GHz, is shown, reporting a change between an optically thick ($\alpha > 0$) and an optically thin ($\alpha < 0$) regime. Such variations could indicate a multiple plasmoid ejection in the jet. In Figure 5, the radio spectrum, as detected by RATAN-600 during the outburst phase (MJD 57198.93), shows a change between an optically thick and an optically thin regime at ~4 GHz.

There is a simultaneity of the peak emission detected by *AGILE* (and *Fermi*-LAT), *INTEGRAL*/SPI (continuum 100–200 keV and annihilation emission), *Swift*/BAT (15–50 keV), and RATAN-600 (2.4–21.7 GHz). The γ-ray flare, detected by the *AGILE*-GRID between 50 and 400 MeV, occurs at MJD 57198.25 ± 1,

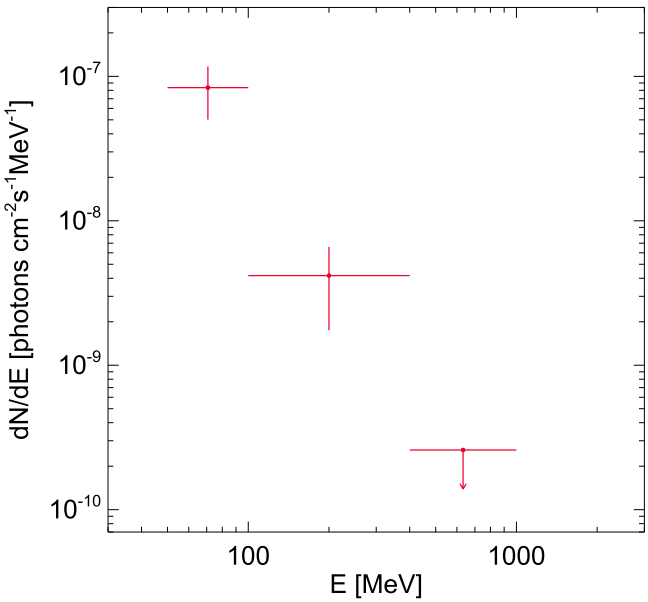

Figure 3. Differential γ-ray spectrum from V404 Cyg as detected by the *AGILE*-GRID during the peak emission activity, 2015 June 24 UT 06:00:00 to 2015 June 26 UT 06:00:00 (MJD 57197.25–57199.25). The flux UL is a 68% C. L. value.

with an integration time including the preparation and prompt phase of the prominent burst detected in radio and hard X-ray frequencies (2015 June 26, MJD 57199). The multiwavelength pattern is very similar to the Cyg X-3 evolution around the γ-ray flare (Fermi LAT Collaboration et al. 2009; Tavani et al. 2009b; Corbel et al. 2012; Piano et al. 2012), and it is consistent with a microquasar behavior, in which transient jets are responsible for the high-energy γ-ray emission (see Section 3.2). While the hard X-ray emission monitored by *Swift*/BAT in the 15–50 keV range is fully dominated by the disk–corona activity, the radio (RATAN-600) and soft/HE γ-ray radiation (*INTEGRAL*/SPI

[10] Public *Swift*/BAT light curves: http://swift.gsfc.nasa.gov/results/transients/weak/V404Cyg/.

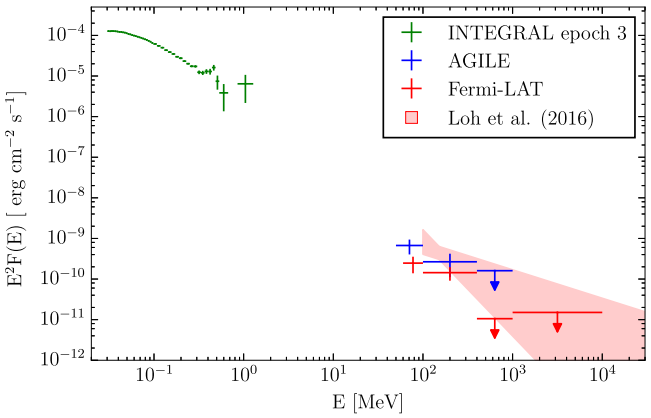

Figure 4. Multifrequency SED of V404 Cyg during the outburst phase. Green points: *INTEGRAL* data, MJD ∼57199.1–57200.9 (epoch 3 in Siegert et al. 2016); blue points: *AGILE* data, MJD 57197.25–57199.25; red points: *Fermi*-LAT data (see the Appendix), MJD 57198.75–59199.75. Red shaded region: 6 hr peak spectrum from Loh et al. (2016), ∼MJD 57199.1–57199.3. The flux ULs are 68% C.L values.

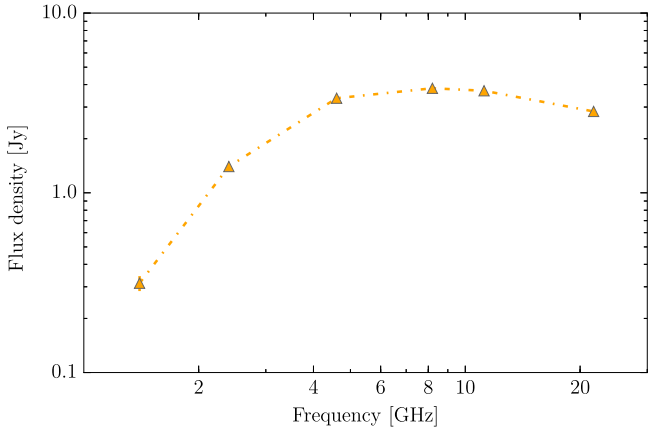

Figure 5. Radio spectrum of the outburst phase (MJD 57198.93) as observed by RATAN-600 (Trushkin et al. 2015).

and *AGILE*-GRID) clearly indicate the presence of a relativistic jet. *INTEGRAL*/SPI detected three time intervals of enhanced continuum emission at 100–200 keV (MJD: ∼57190.9–57192.9, ∼57193.6–57195.6, and ∼57199.1–57200.9). In particular, the second and third intervals show an evident correlation with the 511 keV pair-annihilation emission, suggesting the presence of an unstable antiparticle outflow possibly related to the jet production (Siegert et al. 2016). Radio flux density evolution, as detected by RATAN-600, shows a first peak (∼0.5 Jy at 4.6 GHz) coincident with the second burst activity observed by *INTEGRAL*/SPI (∼57195.0). A giant radio flare (∼3.4 Jy at 4.6 GHz) is detected during the last and brightest peak emission measured by *INTEGRAL*/SPI (∼57199.2), which is consistent with the γ-ray flare detected by the *AGILE*-GRID.

The *AGILE* observations are compatible with the *Fermi*-LAT measurements, reported in Loh et al. (2016) and in the Appendix. The contemporaneous burst observation of V404 Cyg by *AGILE* and *Fermi* gives statistical robustness to this episode, even though the detection significance is not impressive if considered individually. Moreover, the identification of V404 Cyg is secured by the time correlation with a strong outburst detected from the system at other wavelengths.

The multiwavelength behavior suggests that HE γ-ray activity is associated only with the highest activity phase of plasma ejection in the jet. In a jet scenario, the observed HE γ-rays must be produced outside the hot and dense corona region that is opaque (due to $e^+ e^-$ pair production) for photon energies $E \gg m_e c^2$. According to this picture, HE γ-rays produced in the innermost part of the jet are converted to pair plasma. There is a continuous creation and annihilation of plasma close to the central source, forming a broad annihilation line (Loh et al. 2016; Siegert et al. 2016). Outside the coronal plasma, when the plasmoid moves away from the central source along the jet, HE γ-rays can propagate outward without strong absorption (for a quantitative analysis applied to the specific case of Cyg X-3, see Cerutti et al. 2011).

In Figure 4, the spectral energy distribution (SED) at the outburst time is presented, showing *INTEGRAL*, *AGILE*, and *Fermi*-LAT data.

3.2. Microquasar Scenario

As discussed above, the multifrequency emission pattern throughout the outburst clearly resembles the one observed for Cyg X-3 (γ-ray flares detected during X-ray spectral transitions and preceding giant radio outbursts; Corbel et al. 2012; Piano et al. 2012). The peak γ-ray isotropic luminosity for Cyg X-3 was found to be $L_\gamma \sim 10^{36}$ erg s^{-1} (for $E_\gamma \geqslant 100$ MeV and a distance of 7–10 kpc; Fermi LAT Collaboration et al. 2009; Tavani et al. 2009b). It was found that both a leptonic (inverse Compton, IC) and hadronic (π^0-decay) scenario can account for the HE γ-ray emission, although IC processes can explain in a more natural way the γ-ray modulation and the multiwavelength links (Dubus et al. 2010; Piano et al. 2012; Sahakyan et al. 2014).

In V404 Cyg, the simultaneous detection of HE γ-rays, $e^+ e^-$ annihilation emission, and a strong radio outburst can support a microquasar scenario with a dominant leptonic component responsible for the observed pattern of emission (at radio, hard X-ray/soft γ-ray, and HE γ-ray frequencies).

In this work, for V404 Cyg we found a peak γ-ray luminosity $L_\gamma \sim 10^{35}$ erg s^{-1}, for $50 \leqslant E_\gamma \leqslant 400$ MeV and for a source distance of 2.39 kpc. According to the γ-ray observations by *AGILE* and *Fermi*-LAT, $L_\gamma \sim 10^{-4}\, L_{\rm Edd}$ in V404 Cyg, which turns out to be a weaker γ-ray emitter with respect to Cyg X-3. Nevertheless, we have indications of a soft-spectrum HE γ-ray emission with no significant signal observed above 400 MeV. If we take into account the strong emission detected up to soft γ-rays by *INTEGRAL* and compare it with the low significance HE γ-ray flux detected by the *AGILE*-GRID and *Fermi*-LAT, we could ask ourselves whether the bulk γ-ray radiation is concentrated in the energy band between 1 and 50 MeV, a frequency window that current γ-ray detectors cannot observe. By a qualitative extrapolation to this energy range—based on the observed trend (see Figure 4)—we could expect an energy flux around $\sim 10^{-8}$–10^{-6} erg cm^{-2} s^{-1}. Is there a strong energy cutoff in the HE emission (indicating a UL to the Lorentz factor of the emitting particles in the jet)? Is the same spectral component responsible for the hard X-ray and γ-ray radiation? The next generation of γ-ray detectors, such as the e-ASTROGAM space mission (Tatischeff et al. 2016), will be able to explore this energy range with a good sensitivity, trying to disentangle the HE emission scenario for this kind of astrophysical sources.

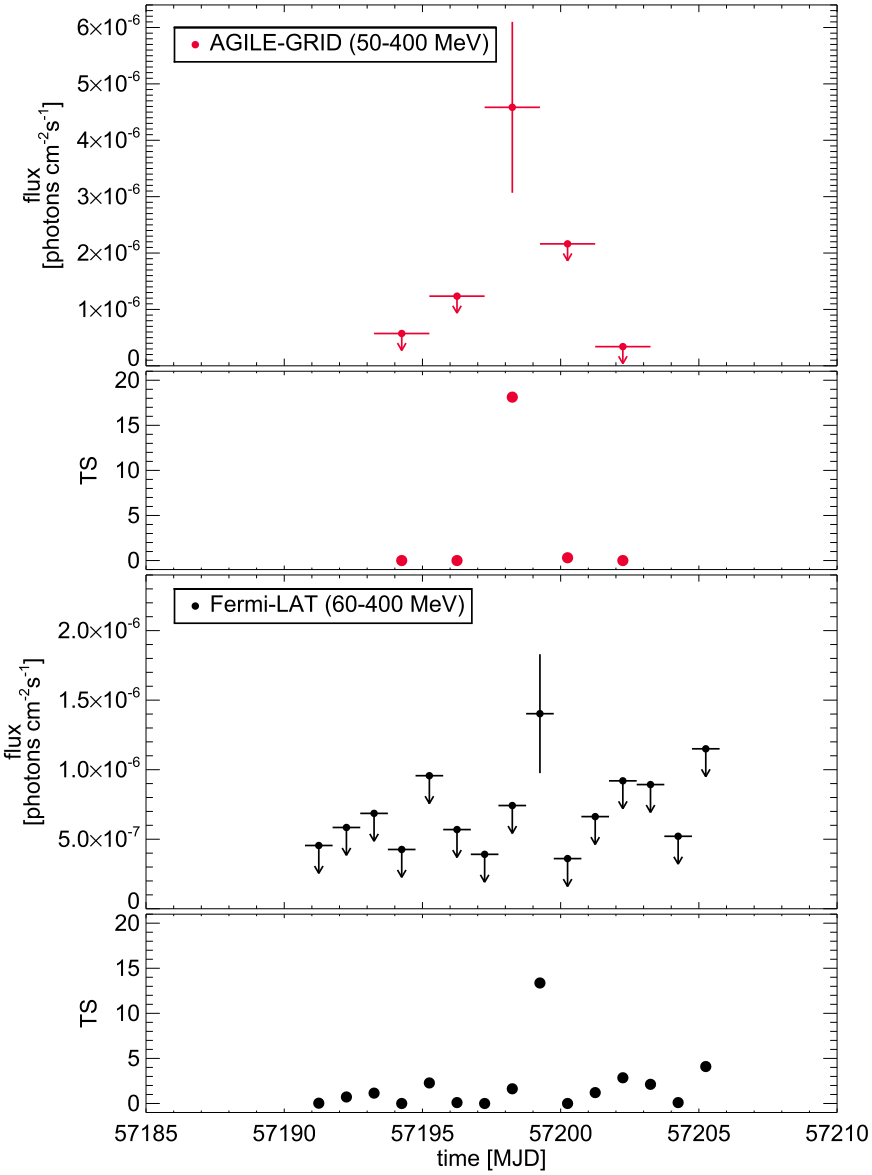

Figure 6. HE γ-ray light curves across the V404 Cyg peak emission. From top to bottom: *AGILE*-GRID 48 hr bin light curve (50–400 MeV energy band); *AGILE*-GRID TS of each time bin; *Fermi*-LAT 24 hr bin light curve (60–400 MeV energy band); *Fermi*-LAT TS for each time bin. For both *AGILE* and *Fermi*, flux error bars and flux ULs are 68% C. L. values.

AGILE is an ASI space mission developed with programmatic support by INAF and INFN. This study was carried out with partial support through the ASI grant No. I/028/12/2.

The authors thank the anonymous referee for stimulating comments on the manuscript and T. Siegert for providing the *INTEGRAL* data shown in Figures 1 and 4 (previously published in Siegert et al. 2016).

The *AGILE* and *Fermi* data behind Figures 1–4 and 6 are provided as supplementary material in a tar.gz archive.

Software: MSLA (Bulgarelli et al. 2012), Fermi Science Tools v10r0p52[11], enrico (Sanchez & Deil 2013).

Appendix
Fermi-LAT Data Analysis

In this appendix, we analyze the *Fermi*-LAT (Atwood et al. 2009) data using the *Fermi* Science Tools `v10r0p5` (see footnote 11) and the user contributed package `enrico`.[12] We analyzed the data between 2015 June 17 UT 18:00:00 (MJD 57190.75) and 2015 July 2 UT 18:00:00 (MJD 57205.75), covering the peak activity period reported at other wavelengths.

We selected data with the `P8R2_TRANSIENT_v16` class in the widest energy range, given the expected faint short-lived activity of this binary in the gamma-ray domain. The data were centered at the position of V404 Cyg and extended within a region of interest of 25° radius. We adopted the last Galactic diffuse emission model (`gll_iem_v06.fits`) and the isotropic model (`iso_P8R2_SOURCE_V6_v06.txt`) in a likelihood analysis, and the 3rd point source catalog `gll_psc_v16.fit` (Acero et al. 2016). In the model, the Galactic diffuse and isotropic components are fixed to the values that we obtained in a long-time integration (one month)

[11] http://fermi.gsfc.nasa.gov

[12] https://github.com/gammapy/enrico/

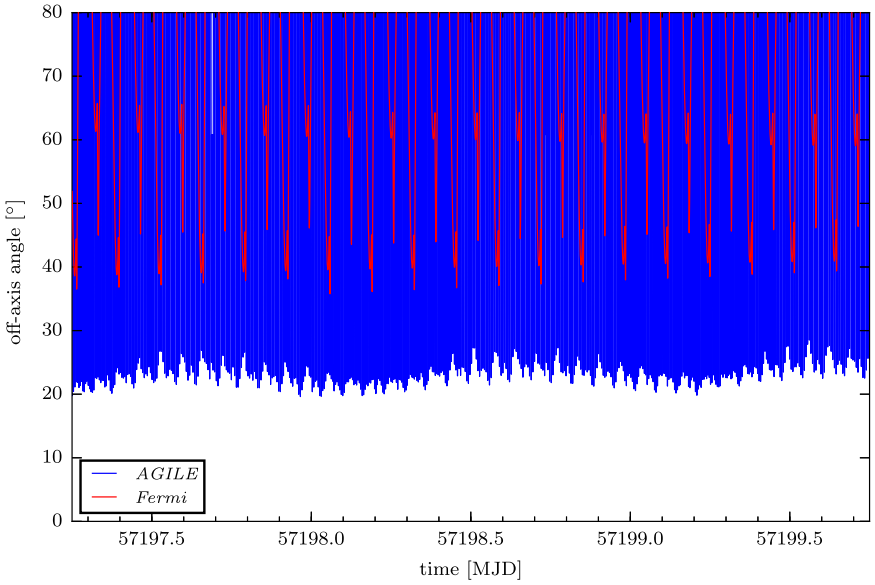

Figure 7. *AGILE*-GRID (blue) and *Fermi*-LAT (red) time evolution of the V404 Cyg off-axis angle, for the period 2015 June 24 UT 06:00:00 and 2015 June 26 UT 18:00:00 (MJD 57197.25–59199.75), union of the γ-ray peak emission time intervals found by *AGILE* and *Fermi* (see Figures 5 and 6).

preceding the active phase of 2015 June . We selected PASS8 FRONT and BACK transient event class. We limited the reconstructed ZENITH_ANGLE to be less than 90° (equivalent to an Earth albedo filtering angle of 75°) to strongly reduce γ-rays coming from the Earth's atmosphere. The good time intervals were selected so that the instrument rocking angle was lower than 52°.

In the data modeling, we took into account nearby sources up to distances of 25°. The analysis procedure was divided into two steps: in the first one, all sources closer than 6° to V404 Cyg had all of their spectral parameters free, while sources further away had their parameters fixed. A likelihood analysis using the Minuit optimizer was run, determining the best-fit parameters for our source and the nearby sources. In a second step, we fixed the spectral parameters for all the sources, except for V404 Cyg, to the ones found in the first step, and ran the likelihood analysis again in order to obtain a refined fit. For V404 Cyg we used a simple power-law model.

We produced light curves with 24 hr time bins in two different energy bands: 60–400 MeV and above 400 MeV. No significant emission was detected above 400 MeV. In the 60–400 MeV light curve, instead, we obtained a hint of a detection at TS = 13.4 ($\sim 3.7\sigma$; see Figure 6) and a γ-ray flux $F_\gamma = (1.4 \pm 0.4) \times 10^{-6}$ photons cm^{-2} s^{-1} for the time integration between 2015 June 25 UT 18:00:00 and 2015 June 26 UT 18:00:00 (MJD 57198.75–59199.75). This result is fully consistent (in flux and integration time) with the 12 hr peak emission found by Loh et al. (2016) in their analysis of the *Fermi*-LAT data in the 100 MeV–100 GeV energy range.

A.1. AGILE–Fermi Comparison

By comparing the *AGILE*-GRID and our independent *Fermi*-LAT analysis, we can note that both γ-ray instruments found a quasi-simultaneous peak emission with a time overlap of 12 hr. The *AGILE*-GRID and *Fermi*-LAT γ-ray fluxes observed at the peak emission are consistent with each other at 2σ C.L.

AGILE and *Fermi* have different sky-scanning strategies and, consequently, they observe the target source at different times and for different duration in every single scan. Thus, if the γ-ray emission time is short (sub-hour variability as in the optical and X-ray frequencies), the detectors can miss part of the peak activity if the source is outside the field of view during the γ-ray activity.

Figure 7 shows the *AGILE*-GRID and *Fermi*-LAT time evolution of the V404 Cyg off-axis angle during the period 2015 June 24 UT 06:00:00 and 2015 June 26 UT 18:00:00 (MJD 57197.25–59199.75), union of the γ-ray peak emission time intervals found by two instruments. As noticed in other studies, *AGILE* and Fermi can have different exposures on a specific target (Sabatini et al. 2013; Munar-Adrover et al. 2016).

References

Acero, F., Ackermann, M., Ajello, M., et al. 2016, ApJS, 223, 26
Atwood, W. B., Abdo, A. A., Ackermann, M., et al. 2009, ApJ, 697, 1071
Barbiellini, G., Fedel, G., Liello, F., et al. 2002, NIMPA, 490, 146
Barthelmy, S. D., D'Ai, A., D'Avanzo, P., et al. 2015, GCN, 17929, 1
Bulgarelli, A., Chen, A. W., Tavani, M., et al. 2012, A&A, 540, A79
Casares, J., & Charles, P. A. 1994, MNRAS, 271, L5
Casares, J., Charles, P. A., & Naylor, T. 1992, Natur, 355, 614
Cerutti, B., Dubus, G., Malzac, J., et al. 2011, A&A, 529, A120
Corbel, S., Dubus, G., Tomsick, J. A., et al. 2012, MNRAS, 421, 2947
Dubus, G., Cerutti, B., & Henri, G. 2010, MNRAS, 404, L55
Fermi LAT Collaboration, Abdo, A. A., Ackermann, M., et al. 2009, Sci, 326, 1512
Hynes, R. I., Bradley, C. K., Rupen, M., et al. 2009, MNRAS, 399, 2239
Jenke, P. A., Wilson-Hodge, C. A., Homan, J., et al. 2016, ApJ, 826, 37
Khargharia, J., Froning, C. S., & Robinson, E. L. 2010, ApJ, 716, 110
Kimura, M., Isogai, K., Kato, T., et al. 2016, Natur, 529, 54
Loh, A., Corbel, S., Dubus, G., et al. 2016, MNRAS, 462, L111
Makino, F., Wagner, R. M., Starrfield, S., et al. 1989, IAUC, 4786, 1
Mattox, J. R., Bertsch, D. L., Chiang, J., et al. 1996, ApJ, 461, 396
Miller-Jones, J. C. A., Gallo, E., Rupen, M. P., et al. 2008, MNRAS, 388, 175
Miller-Jones, J. C. A., Jonker, P. G., Dhawan, V., et al. 2009, ApJL, 706, L230
Munar-Adrover, P., Sabatini, S., Piano, G., et al. 2016, ApJ, 829, 101
Muñoz-Darias, T., Casares, J., Mata Sánchez, D., et al. 2016, Natur, 534, 75
Piano, G., Tavani, M., Vittorini, V., et al. 2012, A&A, 545, A110
Pittori, C., Verrecchia, F., Chen, A. W., et al. 2009, A&A, 506, 1563
Prest, M., Barbiellini, G., Bordignon, G., et al. 2003, NIMPA, 501, 280
Rana, V., Loh, A., Corbel, S., et al. 2016, ApJ, 821, 103
Rodriguez, J., Cadolle Bel, M., Alfonso-Garzón, J., et al. 2015, A&A, 581, L9

Sabatini, S., Donnarumma, I., Tavani, M., et al. 2015, ApJ, 809, 60
Sabatini, S., Tavani, M., Coppi, P., et al. 2013, ApJ, 766, 83
Sahakyan, N., Piano, G., & Tavani, M. 2014, ApJ, 780, 29
Sanchez, D. A., & Deil, C. 2013, arXiv:1307.4534
Segreto, A., Del Santo, M., D'Aí, A., et al. 2015, ATel, 7755
Shahbaz, T., Ringwald, F. A., Bunn, J. C., et al. 1994, MNRAS, 271, L10
Siegert, T., Diehl, R., Greiner, J., et al. 2016, Natur, 531, 341
Tatischeff, V., Tavani, M., von Ballmoos, P., et al. 2016, Proc. SPIE, 9905, 99052N
Tavani, M., Barbiellini, G., Argan, A., et al. 2009a, A&A, 502, 995
Tavani, M., Bulgarelli, A., Piano, G., et al. 2009b, Natur, 462, 620
Trushkin, S. A., Nizhelskij, N. A., & Tsybulev, P. G. 2015, ATel, 7716